(SAE National Aeronautic Meeting, Los Angeles, October 4, 1957)

CORRELATION OF AIRFOIL ICE FORMATIONS AND THEIR AERODYNAMIC EFFECTS WITH IMPINGEMENT AND FLIGHT CONDITIONS

By Vernon H. Gray

National Advisory Committee for Aeronautics
Lewis Flight Propulsion Laboratory
Cleveland, Ohio

Abstract

An empirical equation is developed by which changes in drag coefficients due to ice formations on an NACA 65A004 airfoil may be calculated from known icing and flight conditions; this equation is then extended to include available data for other airfoils up to 15-percent thickness ratio. The correlation was obtained primarily by use of ice heights and ice angles measured on the 4-percent thick airfoil. The final equation, however, does not include the ice measurements, but relates changes in drag coefficients due to ice with the following variables: icing time, airspeed, air temperature, liquid-water content, cloud droplet-impingement efficiencies, airfoil chord, angles of attack, and leading-edge radius-of-curvature,

Changes in lift and pitching-moment coefficients due to ice on an NACA 0011 airfoil are also related to the corresponding changes in drag coefficients; additional data on lift and pitching-moment changes due to ice are limited to the 65A004 airfoil, for which complex trends preclude a relationship within the scope of this paper.

Introduction

In recent years much information about airfoil icing characteristics and their resultant aerodynamic penalties has been acquired by the NACA. This information has been obtained for the five airfoils shown to scale in figure 1. These airfoils have thickness ratios of 4 percent (ref. 1), 9 percent (ref. 2), 11 percent (ref. 3), 12 percent (ref. 4), and 15 percent (unpublished data). In addition, a much larger wealth of information concerning the cloud-droplet impingement characteristics for a variety of airfoils and body shapes has been published. Unfortunately, despite these data, very little direct correlation has heretofore been shown between the aerodynamic penalties due to ice formations, the shape and location of ice formations, and the impingement conditions that produce the ice. Impingement calculations do not quantitatively foretell the size or shape of ice that will form under given conditions, nor are the published aerodynamic penalties related to the actual ice size and shape except in a gross way. Furthermore, it is very difficult to estimate aerodynamic penalties in icing conditions different from those specifically investigated for a particular airfoil.

A review of the aerodynamic data from these previous icing studies showed that, to understand the effects of ice on airfoil characteristics, it would be necessary to study the exact ice shapes and sizes and to relate the aerodynamic effect of the ice to the known effects produced by surface roughness, flow-spoilers, leading-edge flaps, etc, which ice simulates. Such a study has been accomplished with icing data for the NACA 65A004 airfoil section shown in figure 1 (ref. 5). In this

study a variety of ice shapes were accurately measured and related to the generating impingement and icing conditions. The changes in airfoil drag coefficients due to ice were then correlated with the ice shapes and, finally, with impingement and flight conditions. The object of the present paper is to describe this analysis of icing data for the 4-percent thick airfoil and to extend it to include all the airfoil sections for which aerodynamic data in NACA icing tunnel conditions are available.

This investigation was conducted in the NACA Lewis 6- by 9-foot icing tunnel over the following range of variables:

Airfoil thickness ratio, percent	4 to 15
Airfoil angle of attack, deg	0 to 12
Air velocity, mph	Up to 280
Air total temperature, ^{o}F	0 to 30
Liquid-water content, g/cu m	0.25 to 2.0
Volume median droplet diameter, microns	7 to 19
Icing time, min	Up to 27
Pressure altitude, ft	<3500

Owing to the tunnel spray-system design, increases in cloud liquid-water content were accompanied by increases in the droplet size.

Analysis of Ice Shape

The correlation of the aerodynamic effects of ice with its size and shape required accurate measurement of these factors. This measurement was made according to the following techniques.

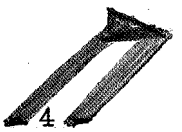

A typical photograph of the cross section of an ice formation at 6° angle of attack is shown in figure 2. After an icing run, the ice on the airfoil was removed by a steam-heated ice scraper except for a narrowband in a chordwise plane normal to the surface. The camera was positioned near the airfoil leading edge and directed spanwise nearly parallel to the leading edge. A black 1/4-inch-mesh wire grid was placed against the ice to provide a scale of measurement, and a white wire of the screen was alined to be an extension of the airfoil chordline. By using a point-plotting procedure with the photographs, two-dimensional cross sections of the various ice formations were made, as shown in the inset of figure 2.

For purposes of analysis, all the cross sections of ice deposits on the 4-percent thick airfoil section were reduced to two significant dimensions, h and θ, as shown in figure 3. Dimension h (in.) is the height of the edge of the ice first reached in going from the upper to the lower surface. The angle 6 (deg) is measured between this ice edge and the extended chordline. The angle is positive if above the chordline and negative if the ice edge falls below the extended chordline.

Representation of ice formations by only these two dimensions ignores the part of the ice toward and on the lower surface of the airfoil. Generally, however, protuberances on this region contribute very little drag to the airfoil, except near 0° angle of attack. In contrast, flow spoilers near the leading edge and toward the upper surface cause large drag increases,

It was found that the dimensions θ and h could each be empirically correlated with the icing test conditions. The resulting correlation for ice angle θ, measured primarily on the 4-percent thick airfoil, is shown in figure 4. In the abscissa of this figure the angle θ is modified by a term which accounts for the airfoil geometric angle of attack at which the ice was formed α_i (deg). The ordinate of figure 4 is a parameter accounting for liquid-water content w (g/cu m), air total temperature t_0 ($^{\circ}$F), and airfoil total droplet-impingement efficiency $\overline{E}_m$. Although considerable scatter of data points exists, the exponents and coefficients of the variables were each adjusted until an equal and minimum scattering of data about an average straight line was obtained.

A convenient scale for representing the types of ice formations (from "rime" to "glaze") is provided by figure 4. The point of demarcation between observed rime and glaze ice deposits lies approximately at a value of 32 on the abscissa scale of figure 4. Ice formations that plot to the left of this point are progressively more rime-like and those to the right are progressively more glaze-like. Thus, use of the ice angle scale in reporting icing conditions or ice types should be more differentiating than use of the general terms rime and glaze.

The ice height h was correlated in a manner similar to that for the angle θ, and the result is shown in figure 5. The ice height h was faund to vary approximately linearly with icing time τ (min) and air velocity V_0 (mph). The term $\overline{\beta}_m$ in the icing parameter of figure 5 is the maximum local droplet-impingement efficiency for the airfoil, and usually occurs very near the leading edge.

Although the correlations developed for θ and h in figures 4 and 5 were based on data for a 6-foot chord, NACA 65A004 airfoil, the relations agree remarkably well with limited unpublished icing data obtained on cylinders and struts of less than 1-inch chord size (square symbols). Therefore, the correlations given for ice height and angle should be valid for a considerable rangecof airfoil shapes and sizes. Thus, with h and θ predictable, and provided airfoil impingement data are available for determining surface limits of impingement (for example, see ref. 6), the aerodynamically significant features of an ice formation can now be composed by calculation.

Correlation Between Ice Shape and Drag

Changes in drag coefficients due to ice formations on the 4-percent thick airfoil section were analyzed on the basis of the ice acting as a leading-edge flap or spoiler. A correlation was obtained utilizing the relations developedin figures 4 and 5 for θ and h, respectively. This correlation is shown in figure 6. The abscissa of figure 6 is the ice angle θ, as determined from the equation of the line given in figure 4. The ordinate of figure 6 is the change in drag caefficient caused by various ice formations corrected to a common height equal to 1 percent of chord $\Delta C_d c/100h$; where c is the airfoil chord (in,), and ΔC_d is the change in the drag coefficient from the clean airfoil value due to the addition of ice. As shown in the ordinate of figure 6, the dimension h is determined from the equation of the line given in figure 5; as a result, figure 6 now expresses the drag changes due

to ice in terms that are either known or calculable in a design or flight performance study.

For clarity, the data points are not shown in figure 6, but instead, the mean curves that describe the trends. Included in the data are several cases in which ice was fomed at an angle of attack α_i and the airfoil was then changed to an angle α, for which C_d was measured and ΔC_d obtained from the clean airfoil drag coefficient at angle α. These data alined themselves very well with the balance of the data taken at fixed angles of attack, corroborating the usefulness of θ in correlating ΔC_d.

Strikingly evident in figure 6 are the reductions in drag coefficients with ice on the airfoil at high angles of attack and low ice angles (rime icing). These dxag reductions below the clean airfoil values are possible because of the high drag coefficients associated with flow separation from thin airfoils with sharp leading edges. The addition of rime ice at the higher angles of attack may at times add bluntness to the airfoil and form a drooped leading edge that assists the flow aver the airfoil nose, and as a result reduces the amount of flow separation from the upper surface. Under glaze icing conditions, however, the ice acts as a flow spoiler and always increases the airfoil drag Coefficients.

Changes in drag coefficients due to ice are shown in figure 6 for each of the geometric angles of attack investigated, An equation has been developed in agreement with the 4-percent thick airfoil data of

figure-6 and which also accounts for variations in the angles of attack from 0° to 12°. This equation is as follows:

$$\Delta C_d \approx \left[8.7\times10^{-5}\frac{\tau V_0}{c}\left(32 - \right)\right]\left[1 + 6\left\{(1+2\sin^4 12\alpha)\sin^2\left[543\sqrt{w}\sqrt[3]{\frac{\bar{E}_m}{32 - t_0}} - 81 + 65.3\left(\frac{\alpha_i}{1.35} - \frac{1}{1.35}\alpha\right)\right] - 1.7\sin^4 11\alpha\right\}\right] \quad (1)$$

The first bracket of equation (1) accounts for the height-to-chord ratio of the significant ice formation, and the last bracket accounts for the ice angle, angle of attack and the case wherein ice is formed at ax).angle of attack different from that under consideration. The term accounting for this latter case vanishes when ice is formed at the same geometric angle of attack as that being considered ($\alpha_i = a$). In the $\sin^2$ function in the last bracket of equation (1) the expression $543\sqrt{w}\sqrt[3]{\frac{\bar{E}_m}{32 - t_0}} - 81$ is valid between the limits of 0 and 180; beyond these limits a value of zero should be used for the expression instead of a calculated number.

Prediction of Drag Changes Due to Ice on Various Airfoils

Having determined equation (1) for approximating the drag coefficient changes due to ice on an NACA 65A004 airfoil, it was desirable to attempt a similar relationship for other airfoils, although ice measurements were available only for the 4-percent thick airfoil, Accordingly, all the applicable NACA icing drag data from references 2, 3, and 4 were inserted into equation (1) for trial, interpolating for impingement

parameters from data of reference 6. These icing data are listed in table I. It was found that an airfoil thickness trend appeared; to account for it, a factor r was introduced, which is the airfoil leading-edge radius-of-curvature in percent of chord. Also, in the absence of more knowledge as to the effect of sweep-back on drag due to ice formations, the 63A009 airfoil (swept 36°) was regarded for correlation purposes the same as an unswept two-dimensional airfoil except that impingement, chord length, and radius-of-curvature were taken for the stream-wise cross section of the airfoil.

A final equation was derived which represents the available icing drag data of the referenced airfoils and which is consistent with equation (1) for the 4-percent thick airfoil:

$$\Delta C_d = \left[8.7\times10^{-5}\,\frac{\tau V_0}{c}\sqrt{w\bar{\beta}_m}\,(32 - t_0)^{0.3}\right]\left[1 + 6\left\{(1 + 2.52r^{0.1}\sin^4 12\alpha)\sin^2\left[543\sqrt{w}\sqrt[3]{\frac{\bar{E}_m}{32 + t_0}} - 81 + 65.3\left(\frac{1}{1.35\alpha_i} - \frac{1}{1.35\alpha}\right)\right] - \frac{0.17}{r}\sin^4 11\alpha\right\}\right] \tag{2}$$

Measured values of ΔC_d from table I and reference 5 are plotted in figure 7 against the calculated values using equation (2). The order of agreement shown in figure 7 appears quite satisfactary, considering the nature and difficulty of obtaining aerodynamic, impingement, and meteorological data in icing conditions.

Estimation of Lift and Pitching-Moment Coefficients

Unfortunately, changes in lift and pitching-moment coefficients due to ice formations are known only for an NACA 0011 airfoil (ref. 3) and an NACA 65A004 airfoil (ref. 1). However, in addition to these data, it should be possible to estimate changes in lift and moment coefficients by utilizing relationahips in the published aerodynamic characteristics of airfoils with and without flaps, spoilers, protuberances, etc.

From the limited data available in icing conditions, it appears that changes in lift and moment coefficients due to ice formations can be related to the concurrent changes in drag coefficients for a thick blunt airfoil such as the 0011 airfail, whereas no systematic relationship is readily apparent for a thin sharp-nosed airfoil such as the 65A004 airfoil. The relationships between changes in lift, moment, and drag coefficients due to ice on the 0011 airfoil are shown in figure 8 as functions of geometric angle of attack, from data of reference 3. Well-established trends are evident in figure 8, wherein increases in drag coefficients are accompanied by similar increases in moment coefficients, and by decreases in lift coefficients of generally larger magnitude. Theae trends are similar to the trends with the 65A004 airfoil, but only up to about 3° angle of attack. At higher angles of attack, changes in lift andmoment coefficients due to ice on the 4-percent thick airfoil were erratic with respect to changes in drag coefficients, due primarily to the flow separation from the upper surface starting at about 4° angle of attack (ref. 1).

Example of Use of Correlation

To illustrate how the preceding correlations may be used to assess the magnitudes of aerodynamic penalties for various airfoils in icing conditions, the following hypothetical icing encounters will be evaluated:

	Icing encounter A	Icing encounter B
Airfoil	658004	65_1-212
Chord, in.	96	240
Angle of attack[a], deg	2	2
Airspeed, mph	500	300
Pressure altitude, ft	8000	8000
Air total temperature, °F	25	10
Liquid-water content, g/cu m	0.5	0.5
Volume-median droplet diameter, microns	15	15
Duration in icing, min	4	7
Clean airfoil drag coefficient[a]	0.0067	0.0088

[a]Corresponding to tunnel geometric angle of attack (uncorrected).

From reference 6 the following impingement parameters may be determined:

	Encounter A	Encounter B
K_0	0.0179	0.00515
$\overline{\beta}_m$	0.67	0.35
$\overline{E}_m$	0.18	0.033

Substitution of the above values in equation (2) yields the following changes in drag coefficients due to the accumulated ice: icing

encounter A, 0.0051, or a 76 percent increase over the clean airfoil drag; icing encounter B, 0.0008, or a 9 percent increase in drag.

If the airfoil angle of attack is increased in a maneuver in clear air up to 8° with the ice formations that accumulated during the preceding encounters at 2° angle of attack remaining where they were formed, the following results are obtained by use of equation (2):

	Icing encounter	
	A	B
Angle of attack at which ice was fomed, deg	2	2
Angle of attack during clear air maneuver, deg	8	8
change in drag coefficient due to ice	0.0127	0.0041
Clean airfoil drag coefficient (at 8°)	0.119	0.0127
Change from clean airfoil drag coefficient, percent increase	10.7	32.3

The 65_1-212 airfoil of encounter B is similar in shape to an NACA 0011 airfoil, so that the relations in figure 8 may be used to estimate the changes in lift and pitching-moment coefficients due to ice accumulated in icing encounter B. These changes are determined from the corresponding changes in drag coefficients previously enumerated, and the ratio factors shown in figure 8. The following results are obtained:

	Icing encounter B	
	Angle of attack	
	2°	8°
Change in lift coefficient	-0.9009	-0.023
Change in moment coefficient	0.0004	0.005
Clean airfoil lift coefficient (typical)	0.35	1.02
Clean airfoil moment coefficient (typical)	-0.035	-0.04
Change from clean airfoil lift coefficient, percent decrease	0.26	2.3
Change from clean airfoil moment coefficient, percent increase (less negative)	1.1	12.5

Changes in lift and pitching-moment coefficients due to ice formations on the 65A004 airfoil of encounter A are not obtainable from the present correlation, but must be estimated from data of reference 1 and related aerodynamic studies of leading-edge spoilers, flaps, etc.

The foregoing examples are typical of calculations that must be made for several representative icing encounters to fully assess the flight penalties due to ice and the need for ice-proteetian equipment.

Conclusion

It should be noted in conclusion that this correlation is a first-order approximation of the presently available aerodynamic and icing data for airfoils exposed to icing conditions in the NACA icing tunnel. Several factors which were thought to be secondary in importance were ignored in this analysis. However, the correlation should be useful in

estimating the type and size of ice formations that would result from *any* specified icing encounter, in estimating the aerodynamic penalties that would result from an encounter, and in making flight performance studies in which icing effects must be evaluated.

References

1. Gray, V. H., and von Glahn, U.: Aerodynamic Effects Caused by Icing of an Unswept NACA 65A004 Airfoil Section. Prospective NACA TN.

2. von Glahn, U. H., and Gray, V. H.: Effect of Ice Formations on Section Drag of Swept NACA 63A-009 Airfoil with Partial-Span Leading-Edge Slat for Various Modes of Thermal Ice Protection. NACA RM E53J30, 1954.

3. Bowden, Dean T.: Effect of Pneumatic De-Icers and Ice Formations on Aerodynamic Characteristics of an Airfoil. NACA TN 3564, 1956,

4. Gray, V. H., and von Glahn, U.: Effect of Ice and Frost Formations on Drag of NACA 65_1-212 Airfoil for Various Modes of Thermal Ice Protection. NACA TN 2962, 1953.

5, Gray, V. H.: Correlations Among Ice Measurements, Impingement Rates, Icing Conditions and Drag Caefficients for an Unswept NACA 65A004 Airfoil Section. Prospective NACA TN.

6. Gelder, T. F., Smyers, W. H,, and von Glahn, U. H: Experimental Droplet Impingement on Several Two-Dimensional Airfoils with Thickness Ratios of 6 to 16 Percent. NACA TN 3839, 1956.

Appendix - Symbols

C_d	airfoil section drag coefficient
ΔC_d	change in section drag coefficient due to addition of ice
ΔC_l	change in section lift coefficient due to addition of ice
ΔC_m	change in section pitching-moment coefficient (about the quarter-chord point) due to addition of ice
c	airfoil chord length, in.
$\overline{E}_m$	total droplet-impingement efficiency (see refs. 5 and 6)
h	height of ice (see fig. 6), in,
K_0	modified inertia parameter (see refs. 5 and 6)
r	radius of curvature of airfoil leading edge, percent of chord
t_0	free-stream total air temperature, ^oF
V_0	free-stream velocity, mph, or knots X 1.15
w	liquid-water content of cloud, g/cu m
a	airfail geometric angle of attack (uncorrected for tunnel walls), deg
α_i	airfoil geometric angle of attack at which ice deposit is formed (uncorrected for tunnel walls), deg
$\overline{\beta}_m$	maximum local droplet-impingement efficiency (see refs. 5 and 6)
τ	icing time, min
θ	ice angle (see fig. 6), deg

TABLE I

NACA airfoil section	Chord length, c, in.	Radius of curvature, r, % chord	Sweep angle, deg	Angle of attack during icing, α_i, deg	Angle of attack, α, deg	Airspeed, V_0, mph	Air total temperature, t_0, °F	Liquid-water content, w, g/cu m	Icing time, τ, min	Airfoil impingement efficiency, $\bar{E}_m$ (a)	Maximum local impingement efficiency, $\bar{\beta}_m$ (a)	Change in drag coefficient due to ice, ΔC_d	Data from ref.
65A004	72	0.10	0	(See refs. 1 and 5 for data)									1, 5
63A009	[b]82.2	0.62	36	2	2	260	25	0.83	15	0.079	0.46	0.0200	2
				4	4	260	25	.83	15	.073	.42	.0230	
				4	4	260	10	.55	15	.057	.38	.0075	
				4	4	260	25	.39	14	.051	.35	.0080	
65_1-212	96	1.00	0	2	2	260	0	0.65	7	0.046	0.43	[c].0004	4
				2	2	260	25	1.40	4	.074	.48	[c].0042	
				2	8	260	25	1.40	5	.074	.48	[c].0370	
				5	5	180	23	1.25	5	.064	.42	[c].0034	
				5	5	260	25	.52	20	.043	.36	.0038	
				5	5	260	0	.70	10	.056	.40	.0017	
0011	87.4	1.30	0	0	0	275	25	0.50	15	0.071	0.51	0.0137	3
				0	0	175	25	.50	16.3	.035	.39	.0038	
				0	0	275	10	.50	27	.072	.51	.0057	
				0	4	175	25	.50	16.3	.035	.39	.0140	
				2	2	275	25	.50	18	.067	.46	.0185	
				2	2	275	25	.70	12.5	.086	.53	.0178	
				2	2	275	10	.65	20	.079	.51	.0092	
				2	2	275	25	.30	18	.038	.35	.0022	
				2	2	175	25	.50	18	.036	.35	.0026	
				2	6	175	25	.50	18	.036	.35	.0096	
				4	4	275	10	.50	10.3	.065	.43	.0046	
				4	4	175	25	1.00	21	.071	.44	.0122	
				4	4	275	25	.50	15.5	.066	.43	.0119	
				6	6	175	25	1.00	12	.075	.43	.0190	
				8	8	175	20	1.00	12.5	.084	.49	.0345	
				8	8	175	25	1.00	8	.082	.47	.0236	
63_1-015	13	1.59	0	4	4	250	10	0.70	5	0.203	0.63	0.0090	Unpublished
				4	4	250	25	.50	10	.222	.66	.0830	

[a]Data interpolated from ref. 6. [b]Stream-wise direction. [c]Cyclic de-icing data.

FIG. 1. NACA AIRFOIL SECTIONS WITH AERODYNAMIC DATA IN ICING CONDITIONS

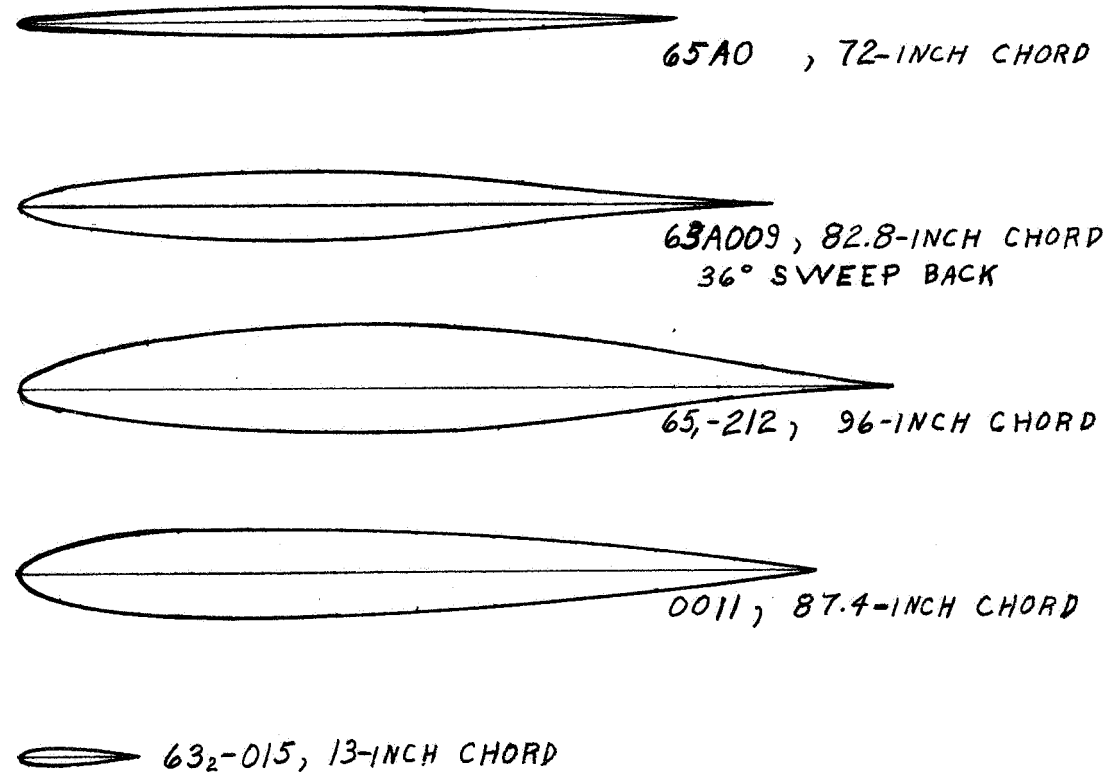

1/20 SCALE

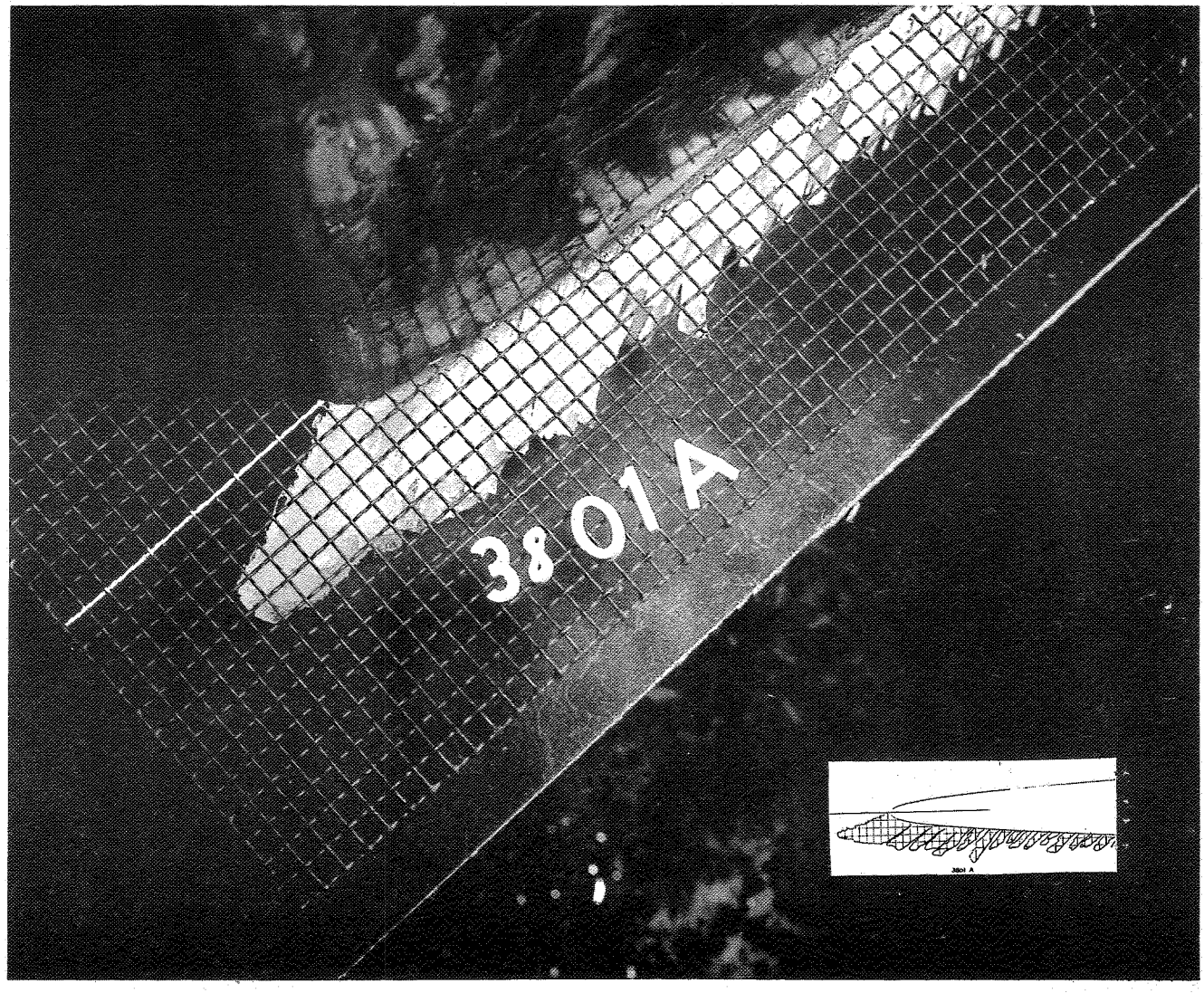

Figure 2 - Typical photograph of ice cross section, with final two-dimensional sketch.

FIGURE 3. REPRESENTATION OF ICE SHAPE BY ANGLE θ AND HEIGHT h.

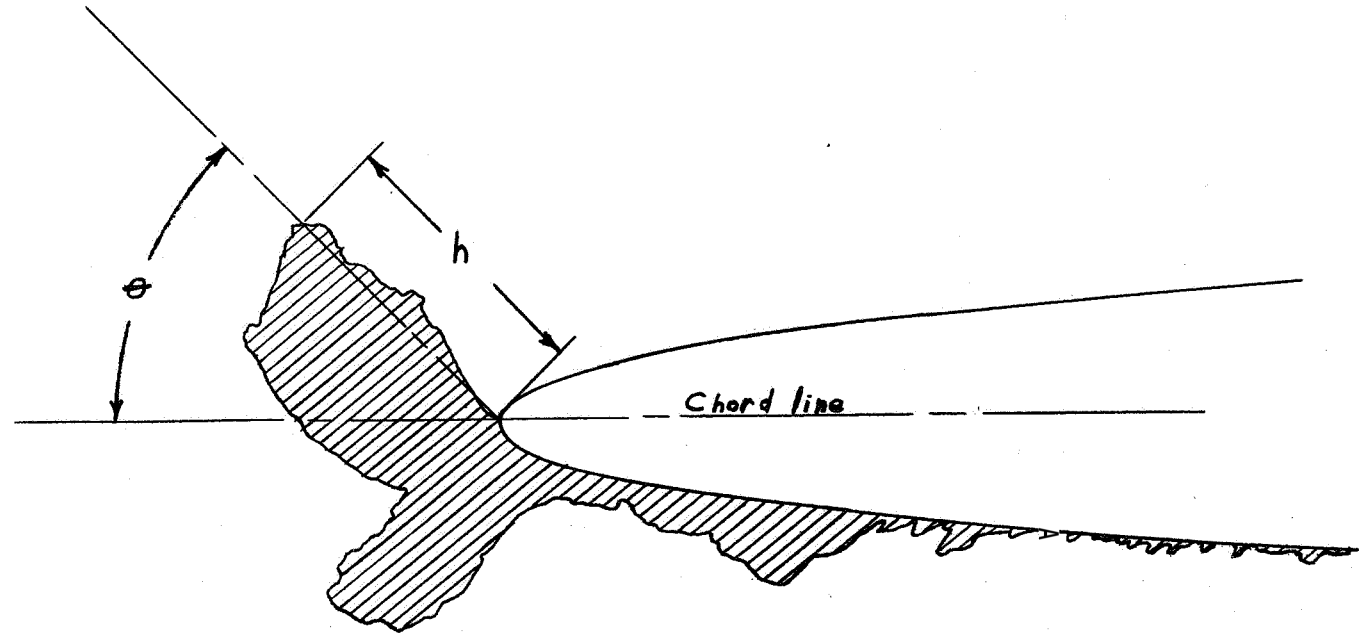

FIGURE 4. CORRELATION OF ICE ANGLE θ WITH ICING CONDITIONS

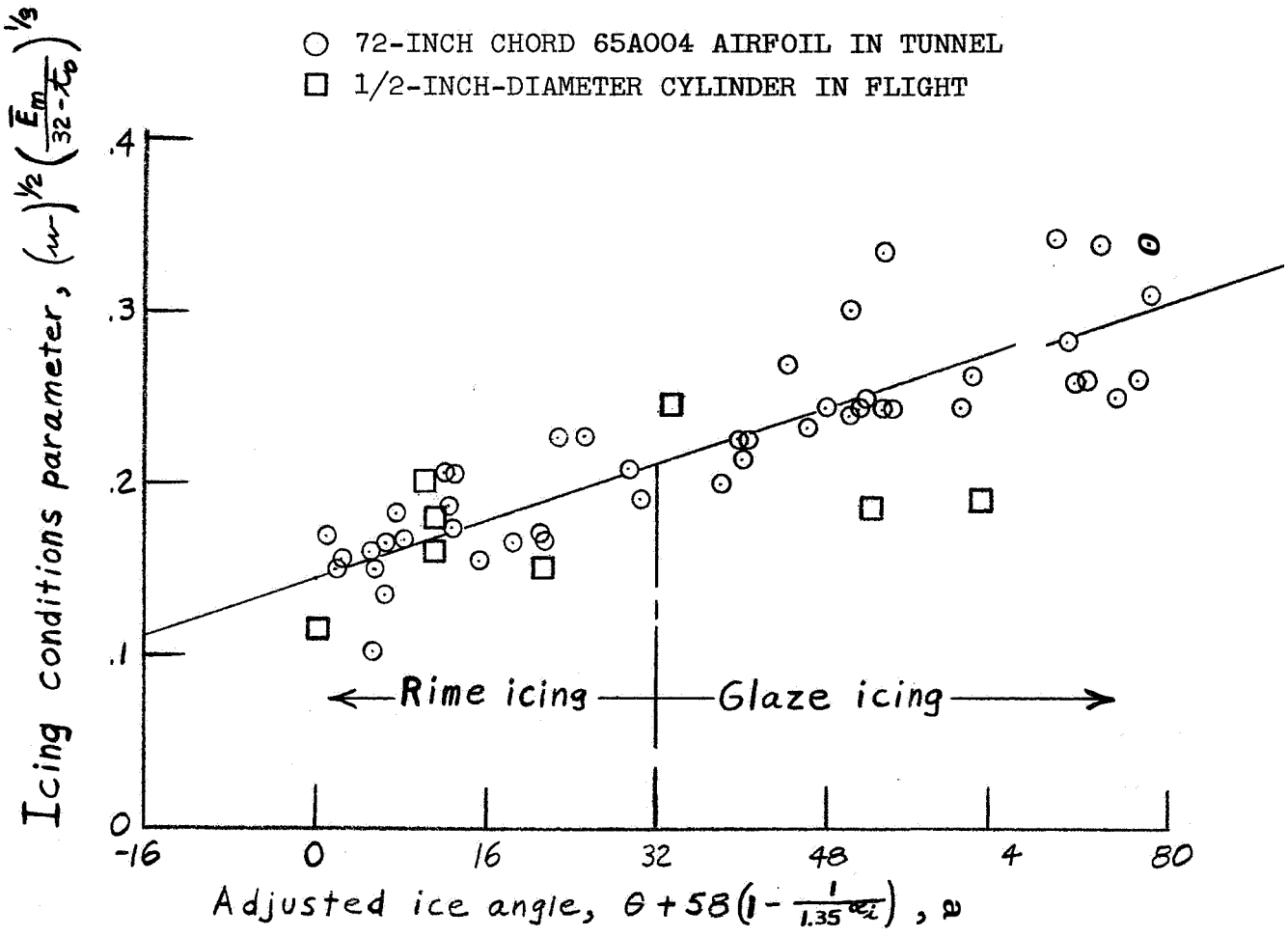

FIGURE 5. CORRELATION OF ICE HEIGHT h WITH ICING CONDITIONS

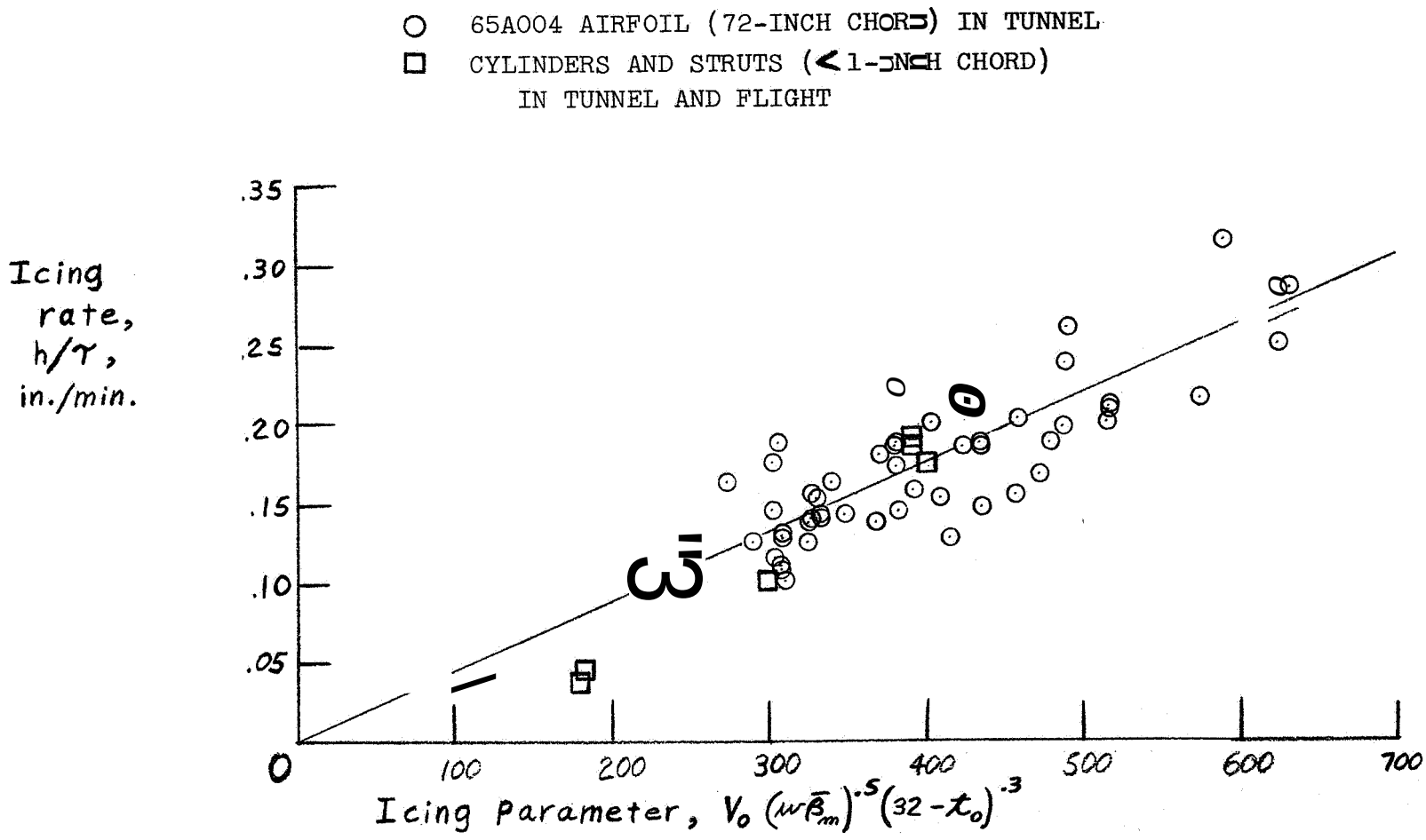

FIGURE 6. CHANGE IN DRAG-COEFFICIENT DUE TO ICE, ΔC_d, AS FUNCTION OF ICE ANGLE θ AND ANGLES OF ATTACK

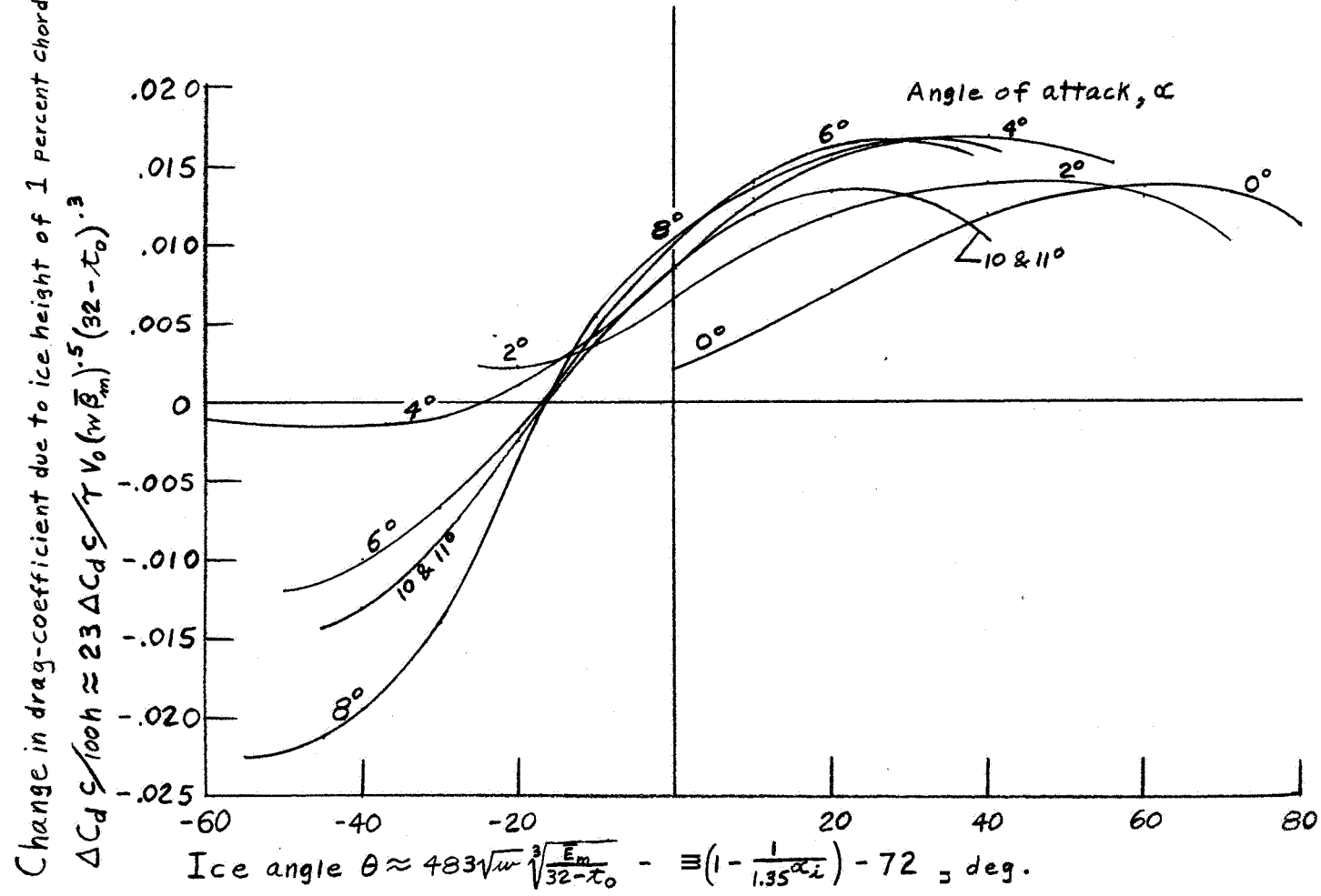

FIGURE 7. COMPARISON OF CALCULATED AND MEASURED ΔC_p

(COMPLETE RANGE OF NACA AIRFOIL ICING DATA)

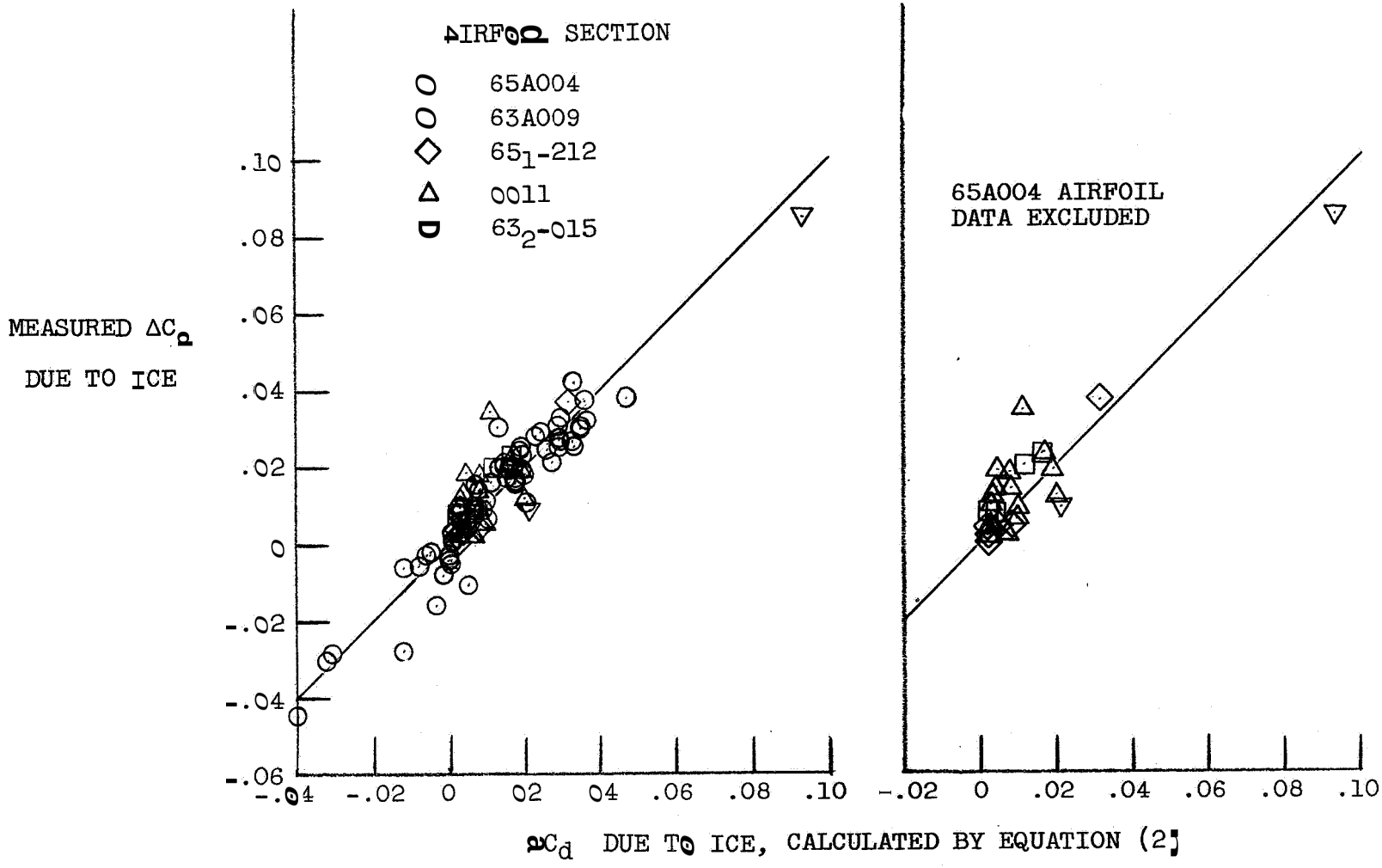

FIGURE 8. CHANGE IN LIFT AND PITCHING MOMENT DUE TO ICE ON 0011 AIRFOIL SECTION
(AS RELATED TO CHANGE IN DRAG)